Supplementary Information

Characterization and isolation of tumor-initiating cells from pancreatic cancer cells

Different laboratories have reported the isolation of tumor-initiating cells (TICs) from pancreatic cancer patients and human pancreatic cancer cell lines (Kim et al, 2011; Li et al, 2007; Rasheed et al, 2010; Simeone, 2008). Most of these studies used distinct surface marker combinations or enzyme-activities to enrich for TICs by cell sorting. The obvious heterogeneity of pancreatic TIC populations and their inconsistent marker profile poses significant problems and limitations for their isolation and analysis. For instance, different groups have isolated distinct, non-overlapping pancreatic TIC subpopulations based on expression of CD44, CD24, ESA, CD133 or high aldehyde dehydrogenase activity (ALDH) (Kim et al, 2011; Li et al, 2007; Rasheed et al, 2010; Simeone, 2008). This obvious heterogeneity can be explained by the existence of distinct subpopulation of rare TICs within the same tumor sample and/or by the mutation status of the tumor cells and cell lines. The latter has been shown to be a critical determinant of the marker combination to be used in order to identify and isolate TICs (Curtis et al, 2010).

The lack of a universal pancreatic TIC marker and the obvious discrepancy of the TIC identity in pancreatic cancer cells prompted us to use in this study a TIC enrichment technique that is based on the growth characteristics of TICs rather than surface marker expression or enzyme activity, i.e. high clonogenic growth and (tumor)sphere formation under non-adherent conditions (Simeone, 2008). For this purpose, we seeded pancreatic cancer cells at low clonal density (10^4 cells per mL) into a 3D soft-agar matrix rather than on non-adherent tissue culture plates. This allowed us to readily, reproducibly and more precisely monitor, quantify and isolate highly clonogenic TICs cells from large spheres (macrospheres) in 3D culture. To demonstrate their tumor initiating capacity in xenograft assays, we isolated single macrospheres from the 3D soft-agar culture by aspiration with a small pipette. The isolation process was monitored under a dissecting microscope. Isolated macrospheres were dissociated into single cell suspensions, counted, re-suspended in 50µL 25 % Matrigel (BD Laboratories) and injected into the lower flanks of nude mice. The limiting dilution *in vivo* tumor growth assay that is generally considered the gold standard for the characterization of TICs, clearly identified the macrosphere forming pancreatic cancer cells as a tumor initiating subpopulation of human pancreatic cancer cells (see manuscript figure 6B). It is also noteworthy that our findings of high level expression of HH ligands (e.g. SHH) in the tumor-initiating macrospheres are consistent with a previous study showing elevated expression of SHH in highly tumorigenic CD24+/CD44+/ESA+ pancreatic cancer cells with TIC/cancer stem cell-like properties (Li et al, 2007).

Furthermore, we cultured TICs from individually isolated macrospheres under 2D adherent conditions for one or more passages before re-seeding 10^4 TIC progeny into 3D matrix cultures or by repeated

alternating cultures in 2D and 3D. Notably, the fraction of macrosphere-forming TICs remained constant (about 1-2%) even after several passages in 2D cultures or serial alternating 2D-3D passages. This suggests that the majority of TIC progeny (98-99%) lose their sphere forming ability when cultured in 2D, but that the rare fraction of clonogenic TICs is maintained in 2D cultures (suppl. information, Figure S8A). Conversely, serial passages (n>2) of TICs in 3D non-adherent cultures led to a significant increase in the number of macrospheres providing additional evidence for their self-renewal capacity (suppl. information, Figure S8B, C).

Histology, immunohistochemistry and Western blot analysis

Skin specimen of mice were fixed over night at 4°C in 4% paraformaldehyde and subsequently embedded in paraffin. Sections were cut on a Leica 250M microtome. Specimen were deparaffinized, stained with hematoxylin/eosin and embedded in HistoFix (Carl Roth Laboratory Equipment). Primary anti-JUN (#9165, Cell Signaling Technology), and anti-human SOX9 (#sc-20095, Santa Cruz Biotechnology) were used at 1:100 dilutions and incubated for 10min at room temperature. Heat induced antigen retrieval was done in EDTA buffer (pH 9.0) (Dako, Denmark). Anti-JUN, anti-SOX9 and anti-CXCR4 antibodies were detected with polymer-based envision reagent (Dako, Denmark) and visualized with DAB. Staining was performed on an automated Autostainer Plus platform (Dako, Denmark). Staining of mouse tissues for Keratin 17 (K17) and Sox9 was done as described previously (Yang et al, 2008).

Western blot analyses were done with the following antibodies:

Antigen	**Cat.No.**	**Manufacturer**	**dilution (1:x)**
EGFR	2232	Cell Signaling Technology	1000
pEGFR (Tyr1068)	3777	Cell Signaling Technology	1000
ERK1/2 (p44/42 MAPK)	9102	Cell Signaling Technology	1000
pERK1/2 (p44/42 MAPK)	9106	Cell Signaling Technology	2000
JUN	sc-1694	Santa Cruz Biotechnology	1000
pJUN (Ser73)	9164	Cell Signaling Technology	1000
β-actin	sc-47778	Santa Cruz Biotechnology	2000
GLI1	2534	Cell Signaling Technology	1000
PARP	9542	Cell Signaling Technology	1000

Luciferase reporter assays

For luciferase reporter assays, HEK293 cells were grown in 24-well CellStar culture plates (Greiner BioOne) at 80% confluency and triple transfected using Transfectin (Bio-Rad) with effector expression vector, the respective luciferase reporter plasmid and a β-galactosidase expression vector (pcDNA4/TO/lacZ; Invitrogen) for normalization. As negative control empty pcDNA4/TO vector (Invitrogen) was transfected. Luciferase activity was measured 48 hours after transfection with a luminometer (Lucy 2, Anthos) using Luciferase Assay Substrate (Promega) according to the manufacturer's instructions. Data were normalized for β-galactosidase activity using *ortho-*

nitrophenyl-β -galactoside (ONPG; Sigma Aldrich) as substrate. LacZ activity was quantified by measuring absorbance at 405 nm.

Additional information on *K5cre;Cleg2* mice

K5cre mice (Ramirez et al, 2004) express Cre recombinase under the Keratin 5 promoter, driving Cre expression in the basal layer of the epidermis and in the outer root sheath of hair follicles. *Cleg2* mice (Pasca di Magliano et al, 2006) express dominant active human GLI2 (GLI2deltaN) in response to cre-mediated deletion of a floxed EGFP stop cassette. *K5cre;Cleg2* mice develop macroscopic skin tumors at the age of 5-6 weeks and die around 8 weeks after birth.

References

Curtis SJ, Sinkevicius KW, Li D, Lau AN, Roach RR, Zamponi R, Woolfenden AE, Kirsch DG, Wong KK, Kim CF (2010) Primary tumor genotype is an important determinant in identification of lung cancer propagating cells. Cell Stem Cell 7**:** 127-133

Kasper M, Schnidar H, Neill GW, Hanneder M, Klingler S, Blaas L, Schmid C, Hauser-Kronberger C, Regl G, Philpott MP et al (2006) Selective modulation of Hedgehog/GLI target gene expression by epidermal growth factor signaling in human keratinocytes. Mol Cell Biol 26**:** 6283-6298

Kim MP, Fleming JB, Wang H, Abbruzzese JL, Choi W, Kopetz S, McConkey DJ, Evans DB, Gallick GE (2011) ALDH activity selectively defines an enhanced tumor-initiating cell population relative to CD133 expression in human pancreatic adenocarcinoma. PLoS One 6**:** e20636

Li C, Heidt DG, Dalerba P, Burant CF, Zhang L, Adsay V, Wicha M, Clarke MF, Simeone DM (2007) Identification of pancreatic cancer stem cells. Cancer Res 67**:** 1030-1037

Pasca di Magliano M, Sekine S, Ermilov A, Ferris J, Dlugosz AA, Hebrok M (2006) Hedgehog/Ras interactions regulate early stages of pancreatic cancer. Genes Dev 20**:** 3161-3173

Ramirez A, Page A, Gandarillas A, Zanet J, Pibre S, Vidal M, Tusell L, Genesca A, Whitaker DA, Melton DW et al (2004) A keratin K5Cre transgenic line appropriate for tissue-specific or generalized Cre-mediated recombination. Genesis 39**:** 52-57

Rasheed ZA, Yang J, Wang Q, Kowalski J, Freed I, Murter C, Hong SM, Koorstra JB, Rajeshkumar NV, He X et al (2010) Prognostic significance of tumorigenic cells with mesenchymal features in pancreatic adenocarcinoma. J Natl Cancer Inst 102**:** 340-351

Simeone DM (2008) Pancreatic cancer stem cells: implications for the treatment of pancreatic cancer. Clin Cancer Res 14**:** 5646-5648

Yang SH, Andl T, Grachtchouk V, Wang A, Liu J, Syu LJ, Ferris J, Wang TS, Glick AB, Millar SE et al (2008) Pathological responses to oncogenic Hedgehog signaling in skin are dependent on canonical Wnt/beta3-catenin signaling. Nat Genet 40**:** 1130-1135

Table S1: GLI1/2 Regulated Cell Cycle Gene Expression				
Gene Symbol	fold change by GLI1	StdDev	fold change by ΔNGLI2	StdDev
CDT1*	11.55	1.81	9.57	1.4
ORC1L*	8.23	1.86	7.11	0.87
ORC2L	0.66	1.51	1.17	0.09
CDC6	8.39	0.45	7.23	0.71
MCM2*	6.57	1.24	5.19	0.13
MCM3	3.53	0.25	3.36	0.22
MCM4	3.37	0.3	2.74	0.27
MCM5*	4.67	0.59	5.21	0.64
MCM6*	11.59	0.61	6.51	0.64
MCM7*	6.93	0.98	5.96	0.15
MCM8	2.82	0.48	3.03	0.13
UBE1	1.15	0.07	1.04	0.11
CDK4	1.56	0.33	1.84	0.13
ABL1	1.18	0.13	1.26	0.15
CDKN3*	5.86	1.17	5.41	0.92
CUL1	1.13	0.11	-0.17	2.05
CUL2	0.48	1.38	1.19	0.04
RPA3	1.42	0.21	2.08	0.2
SUMO1	1.18	0.16	1.34	0.1
CCND1*	1.4	0.14	1.94	0.19
CCND2	-1.45	0.11	-1.46	0.07
CCND3	-1.66	0.09	0.02	1.6
PCNA	-0.46	1.3	1.35	0.23
WEE1	3.25	1.22	3.26	0.32
PLK1*	4.53	0.77	5.87	0.57
ANAPC2	-1.29	0.29	0.17	1.7
BCCIP	-0.42	1.29	-1.17	0.09
CCNB1	5.56	0.7	6.58	2.81
CCNB2*	8.34	1.2	11.17	3.24
CCNG1	1.1	0.15	-0.18	1.67
CCNG2	-0.5	1.45	0.06	1.54
CCNT1	-0.4	1.35	1.07	0.05
CCNT2	-0.4	1.34	1.29	0.25
CKS1B*	3.33	1.76	4.23	0.52
HERC5	1.71	0.35	3.14	0.15
CCNH	0.38	1.23	-1.25	0.09
CDK7	0.53	1.42	1.19	0
CDK8	0.19	1.57	-0.06	1.54
CCNF*	3.3	0.38	4.01	0.39
CDC2	9.44	1.97	10.14	2.22
CDC16	-1.2	0.19	0.02	1.49
MRE11A	1.53	0.06	1.44	0.18
RAD51*	7.64	0.31	6.03	1.32
Aurora B*	8.85	1.48	6.5	0
INCENP	2.33	0.2	2.18	0.05
CENPA*	9.75	0.71	9.03	0.22
CENPB	1.29	0.07	0.04	1.63
CDKN2A	-0.43	1.1	0.1	1.66
CDKN2B	-3.83	0.3	-4.86	0.59
CHEK1*	5.66	1.06	5.39	0.66
CHEK2	0.57	1.39	1.44	0.04
CDC34	0.35	1.33	-1.33	0.42
KNTC1*	4.38	0.78	4.21	0.1
CDKN1A	-3.34	0.36	-4.09	0.5
CDKN1B	1.82	0.51	2.24	0.44
CDKN1C	-1.91	0.14	-6.28	1.67
CDC25B	1.95	0.3	2.69	0.07
FOXM1*	12.93	1.8	13.32	2.27
SKP2	1.83	0.55	1.84	0.13
CCNC	0.47	1.42	-0.02	1.65
CDC45L*	19.14	6.12	9.85	0.87
CCNA2	8.89	0.52	8.02	0.78
CCNE1	3.06	0.72	1.28	0.06
TOPBP1*	4.25	0.5	5.21	0.48
CDK3	1.53	0.29	-1.13	0.08
CDC20	9.24	2.72	9.14	2
CDKN5R1	1.26	0.24	1.22	0.27
E2F1*	8.64	1.35	6.46	1.41
E2F2	-1.33	0.29	-1.19	0.12
E2F3	1.72	0.33	1.37	0.07
E2F4	-0.41	1.43	-0.02	1.54

Table S1: Regulation of cell cycle genes by GLI1 and GLI2. Numbers represent fold change values of GLI1 or dominant active GLI2 (ΔNGLI2) expressing HaCaT keratinocytes compared to GLI-negative HaCaT cells as determined by qPCR analysis. Cells were treated with doxycycline to induce GLI1/ΔNGLI2 expression or control treated (solvent only) for 48 hours before analysis. Values represent the mean of three independent experiments. Asterisks indicate cell cycle regulators with putative GLI binding sites in their respective *cis*-regulatory regions as determined by *in silico* promoter screening (see Table S2). Hh/Gli mediated regulation of cell cycle genes with putative GLI binding sites was validated also in mouse cerebellar granular precursor cultures treated with Sonic Hh (data not shown).

Table S2: in silico Gli binding site prediction			
Gene Symbol	putative Gli binding site	position rel. to TSS	reference
CDT1*	gaccacccg	-769	(Ikram et al. 2004)
	gatcaccca	-2098	(Kasper et al. 2006)
ORC1L*	cgccaccca	-1267	(Regl et al. 2004)
MCM2*	gcccaccca	-3794	(Yoon et al. 2002)
	caccaccca	-4845	(Yoon et al. 2002)
MCM5	gacctccca	-2600	(Yoon et al. 2002)
MCM6	caccaccca	-4803	(Yoon et al. 2002)
	gacctccca	-1124	(Yoon et al. 2002)
MCM7*	gaccaccaa	-1973	(Winklmayr et al., 2010)
	gcccacccg	-1264	(Eichberger et al. 2004)
CDKN3	gaccaccca	-3208	(Kinzler et al. 1990)
	gcccaccca	-2358	(Yoon et al. 2002)
	gcccaccca	-2343	(Yoon et al. 2002)
	gcccacccg	-3495	(Eichberger et al. 2004)
	caccacccg	-3560	(Kasper et al. 2006)
	caccgccca	-4013	(Teh et al. 2002, Kasper et al. 2006)
CCND1*	gacctccca	-4520	(Yoon et al. 2002)
	gcccacccg	-3685	(Eichberger et al. 2004)
	gcccacccg	-3125	(Eichberger et al. 2004)
	caccacccg	-2755	(Kasper et al. 2006)
Plk1	gacctccca	-3071	(Yoon et al. 2002)
CCNB2	gcccaccca	-296	(Yoon et al. 2002)
	caccgccca	-4807	(Teh et al. 2002, Kasper et al. 2006)
CKS1B	tgccaccca	-2865	(Kasper et al. 2006)
CCNF	gcccaccca	-4643	(Yoon et al. 2002)
	gcacaccca	-2079	(Regl et al. 2004)
RAD51	gacccccca	-4135	(Yoon et al. 2002)
Aurora B	gaacaccca	1737	(Sasaki et al. 1997)
	tgccaccca	-3361	(Kasper et al. 2006)
CENPA	caccgccca	502	(Teh et al. 2002, Kasper et al. 2006)
CHEK1	caccgccca	-746	(Teh et al. 2002, Kasper et al. 2006)
KNTC1*	gaacaccca	-200	(Sasaki et al. 1997)
	gacctccca	1379	(Yoon et al. 2002)
	gatcaccca	1938	(Kasper et al. 2006)
FOXM1*	gcccaccca	-232	(Yoon et al. 2002)
	gaccgcaca	-110	unpublished
CDC45L*	ggacaccca	-1223	unpublished
TOPBP1*	caccaccca	-4171	(Yoon et al. 2002)
	gacctccca	-4584	(Yoon et al. 2002)
	gcccacccg	196	(Eichberger et al. 2004)
	caccgccca	-207	(Teh et al. 2002, Kasper et al. 2006)
E2F1*	gaccacaca	-1287	(Winklmayr et al., 2010)
	gaccaccct	-1457	(Winklmayr et al., 2010)

Table S2: *In silico* identification of putative GLI binding sites in GLI-regulated cell cycle genes. The GLI binding site sequences and their location relative to the transcriptional start site are shown. Cell cycle genes with GLI binding sites labeled with an asterisk were selected for further analysis by chromatin immunoprecipitation analysis. Selection criteria were sequence, number and clustering of putative GLI binding sites.

Table S3: Primer sequences for qPCR and ChIP analysis

Gene	Forward primer (5´-3´)	Reverse primer (5´-3´)	amplicon length
qPCR human			
IL1R2	CCATGAAGGCCAGCAATACCACATCAC	CGGGATTGTCAGTCTTGACCCCAGA	136bp
PTCH	TCCTCGTGTGCGCTGTCTTCCTTC	CGTCAGAAAGGCCAAAGCAACGTGA	200bp
CD133	AAAGTGGCATCGTGCAAACCTGTGG	TCATCGTACACGTCCTCCGAATCCA	200bp
NANOG	GGGGTTTCACTGTGTTAGCCAGGATGG	GCCAGAGACGGCAGCCAAGGTTATT	150bp
OCT4	AAACGACCATCTGCCGCTTTGAGG	TCCAGGTTGCCTCTCACTCGGTTCT	196bp
GLI1	TCTGGACATACCCCACCTCCCTCTG	ACTGCAGCTCCCCCAATTTTTCTGG	191bp
SHH	TGATGAACCAGTGGCCAGGAGTGA	ACCGAGCAGTGGATATGTGCCTTG	217bp
IHH	GCGCCGACCGCCTCATGACC	TCTGATGTGGTGATGTCCACCG	178bp
DHH	GGAGAGGGAGGGGGAGGGAGAAAAT	TTAGCCTCTCCCCCAGTGCTTCAGC	150bp
JUN	AGTGCGATGTTTCAGGAGGCTGGAG	TTCTCAAAGCAGGAATTGGTGGCAGA	177bp
SOX9	CCTCCTGCCTTTGCTTGTTCACTGC	CTCGGGCACTTATTGGCTGCTGAAA	106bp
FGF19	AGGAGATCCGCCCAGATGGCTACAA	GCAGCATGGGCAGGAAATGAGAGAG	138bp
TGFA	CGCCCTGTTCGCTCTGGGTATTG	CGGTGATGGCCTGCTTCTTCTGG	281bp
SPP1	GCCAGCAACCGAAGTTTTCACTCCA	GCACCATTCAACTCCTCGCTTTCCA	183bp
CXCR4	GGTGGTCTATGTTGGCGTCT	TGGAGTGTGACAGCTTGGAG	227bp
SOX2	GAAATGGGAGGGGTGCAAAAGAGGA	CGTGAGTGTGGATGGGATTGGTGTT	146bp
RPLP0	GGCACCATTGAAATCCTGAGTGATGTG	TTGCGGACACCCTCCAGGAAGC	215bp
qPCR mouse:			
Rplp0	TGCACTCTCGCTTTCTGGAGGGTG	AATGCAGATGGATCAGCCAGGAAGG	193bp
Ptch	CTGTGCCTGTGGTCATCCTGATTGC	CAGAGCGAGCATAGCCCTGTGGTTC	119bp
Gli1	CACCGTGGGAGTAAACAGGCCTTCC	CCAGAGCGTTACACACCTGCCCTTC	191bp
Sox2	CTACATGAACGGCTCGCCCACCTAC	CTGGCCTCGGACTTGACCACAGAG	102bp
Sox9	AGGGCTACGACTGGACGCTGGTG	TGTAATCGGGGTGGTCTTTCTTGTGCT	273bp
Spp1	TCGTCCCTACAGTCGATGTCCCCAAC	CCTGATCAGAGGGCATGCTCAGAAGC	207bp
cJun	AGCGTCCCCCTCCCCCTCAC	CCCGCAGACCAGTCCCAGCA	144bp
Tgfa	GCCAGCCAGAAGAAGCAAGCCATC	GAGGGCACGGCACCACTCACA	132bp
Egfr	AGGGCTATCTGGTGAACGCATCTGG	TGGCGTGGCATAGGTGGCAGA	240bp
Lgr5	GATGCTGCTCAGGGTGGACTGCTC	GGCGATGTAGGAGACTGGCGGGTAG	131bp
Nanog	AGGGCTATCTGGTGAACGCATCTGG	AAGTTATGGAGCGGAGCAGCATTCC	169bp
Cxcr4	CATCCTTTTGGGGGTCATCAAGCAAG	TGGGGTTCAGGCAACAGTGGAAGA	107bp
Il1r2	AGATGAGCCAAGGATGTGGGTGAAGG	CGGTGGTGGAGAGAGCTGAGATTTGC	200bp
ChIP analysis	**Foward primer (5`-3`)**	**Reverse primer (5´-3´)**	
RPLP0	AACGCGAGGCAGCGCCTTCCTTC	TCCATGCTTCCCGCCGGCGAC	284bp
PTCH	GAGGATGCACACACTGGGTTGCCTA	GGGCTGTCAGATGGCTTGGGTTTCT	148bp
CCND1	CAGGGAAGGAGTATGTTCGGCACCA	CAGGGAAGGAGTATGTTCGGCACCA	129bp
CDT1	CGCTTTGGGAGGGGGCAGTTC	CACTCCAGCCTGGGCGACAGC	143bp
FOXM1	CGTCCCCAAACTCTCCCTCGGCT	CTTGTCTCGGCATTCCGGGCTC	178bp
KNTC1	CGAGGCGGTGATTGGGTGTTCTTT	CGCATTCCGGGGGTGTATTCTTG	83bp
TOPBP1	CCCAGCAAAGCCCTAAACCCAAAGG	CAGCAGAAGAGCGGAAATGTCAAACG	104bp

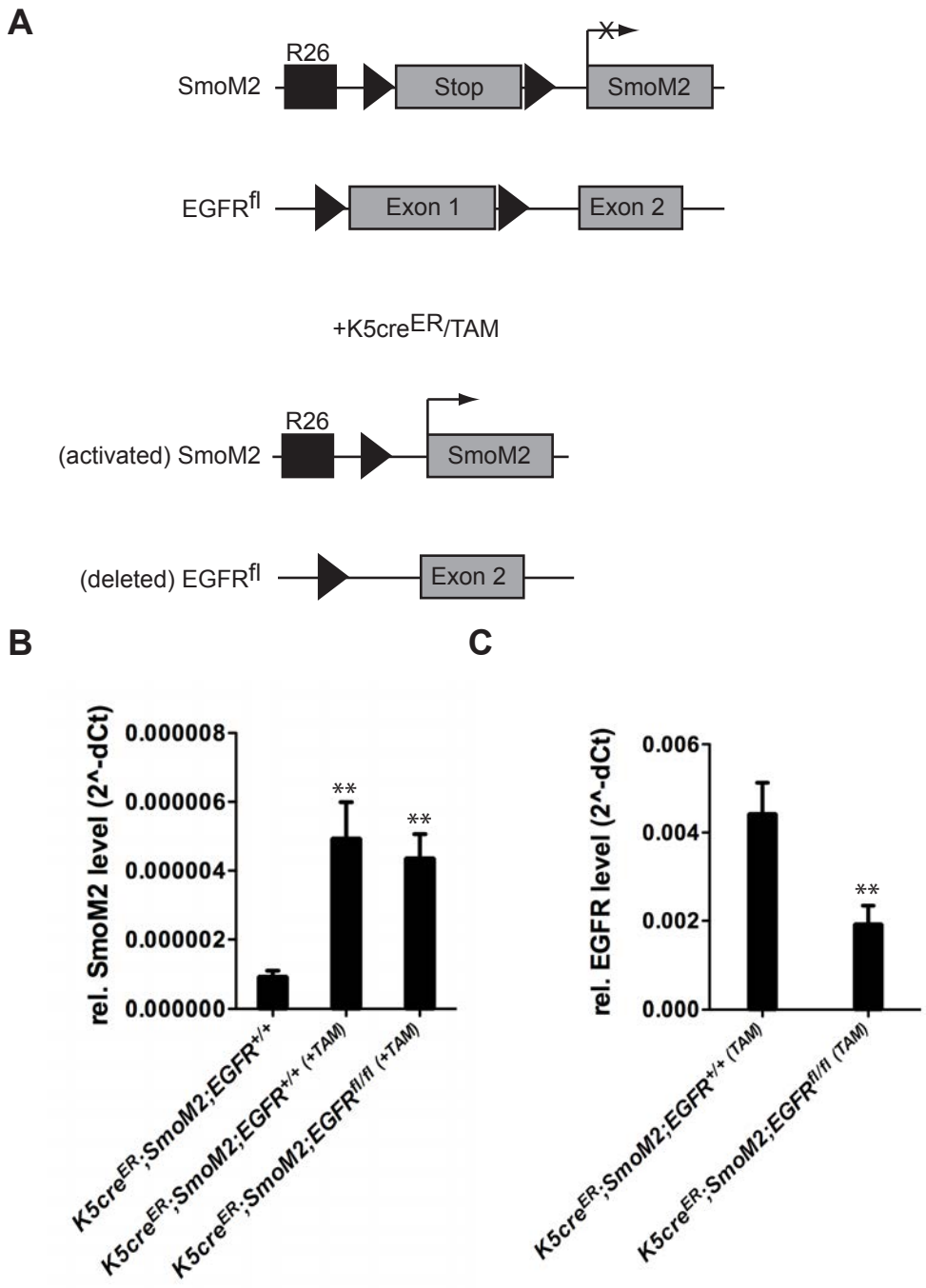

Figure S1: Mouse model of BCC and epidermal specific deletion of EGFR. A) *SmoM2* mice carry a conditional allele of an oncogenic Smoothened variant (SmoM2) that is expressed from the Rosa26 (R26) locus in response to Cre recombinase activity, which deletes the floxed Stop cassette 5´ of the SmoM2 oncogene. Inactivation of EGFR is accomplished by Cre-mediated deletion of floxed Exon1 of $EGFR^{fl}$ mice. LoxP sites are illustrated by black triangles. For epidermal-specific activation of SmoM2 expression and ablation of EGFR function, respectively, we bred $K5cre^{ER}$ mice expressing tamoxifen-regulated Cre recombinase in the basal layer of the epidermis and the outer root sheath of hair follicles with *SmoM2* and $EGFR^{fl/fl}$ or $EGFR^{+/+}$ mice for controls. This yielded $K5cre^{ER}$;*SmoM2*;$EGFR^{+/+}$ and $K5cre^{ER}$;*SmoM2*;$EGFR^{fl/fl}$ mice. Activation of Cre recombinase was done by i.p. tamoxifen (TAM) administration. B) qPCR mRNA expression analysis showing successful activation of SmoM2 expression (left graph) and inhibition of EGFR expression in keratinocytes of transgenic mice. Error bars represent SEM. ** = $p<0.01$;

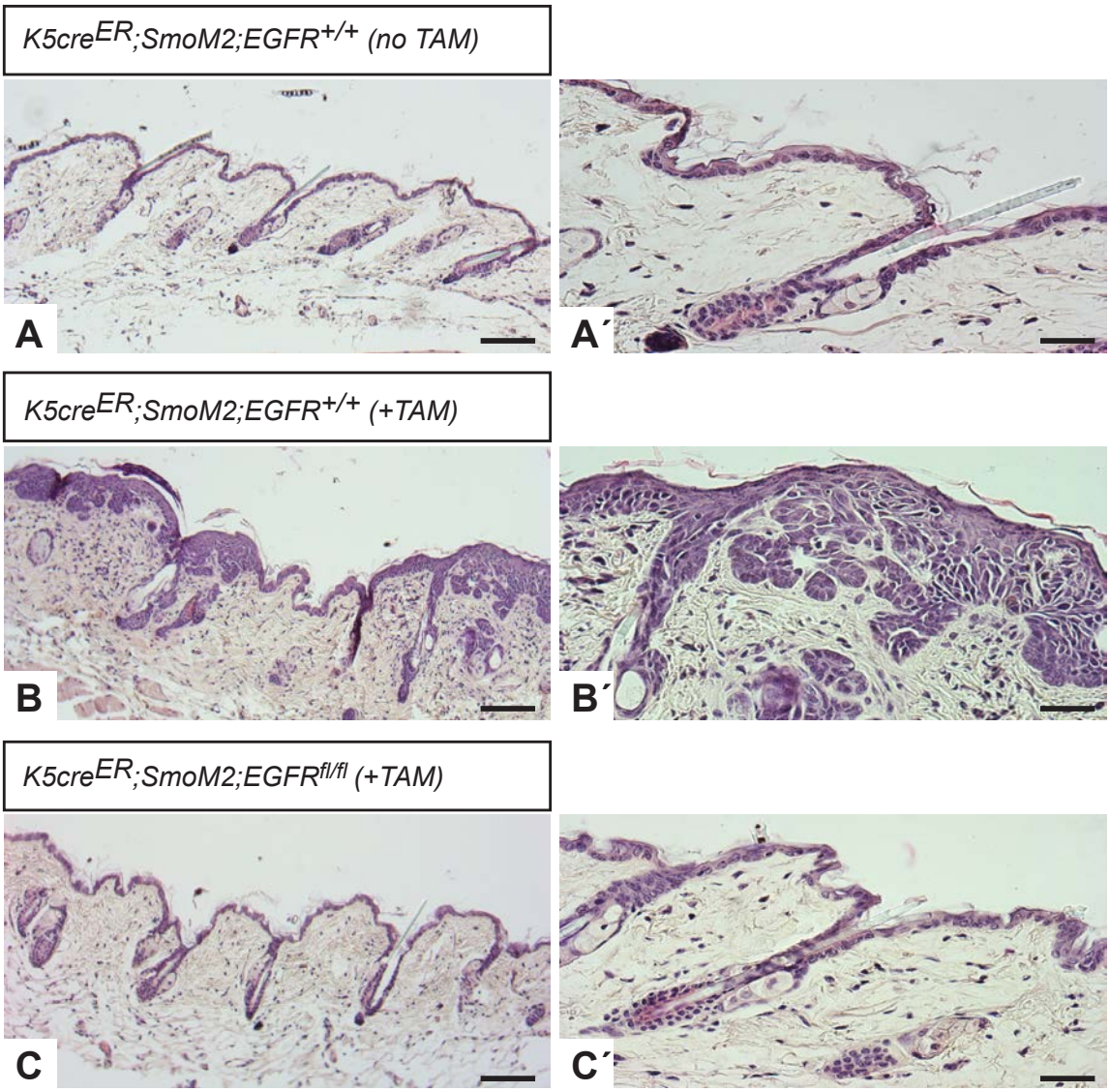

Figure S2: Epidermal-specific deletion of EGFR inhibits the development of SmoM2-driven tumor lesions in dorsal skin. A-A´) Wild-type dorsal skin phenotype of *K5cre^{ER};SmoM2;EGFR$^{+/+}$* mice without tamoxifen (-TAM). B-B´) Activation of epidermal-specific SmoM2 expression by tamoxifen (+TAM) induces basaloid hyperplasia and basaloid hamartoma-like lesions in dorsal skin. C-C´) Conditional deletion of EGFR by tamoxifen administration (+TAM) to *K5cre^{ER};SmoM2;EGFR$^{fl/fl}$* mice prevents SmoM2-driven tumor development in dorsal skin. Scale bar in A, B, C: 400µm, in A´, B´, C´: 100µm

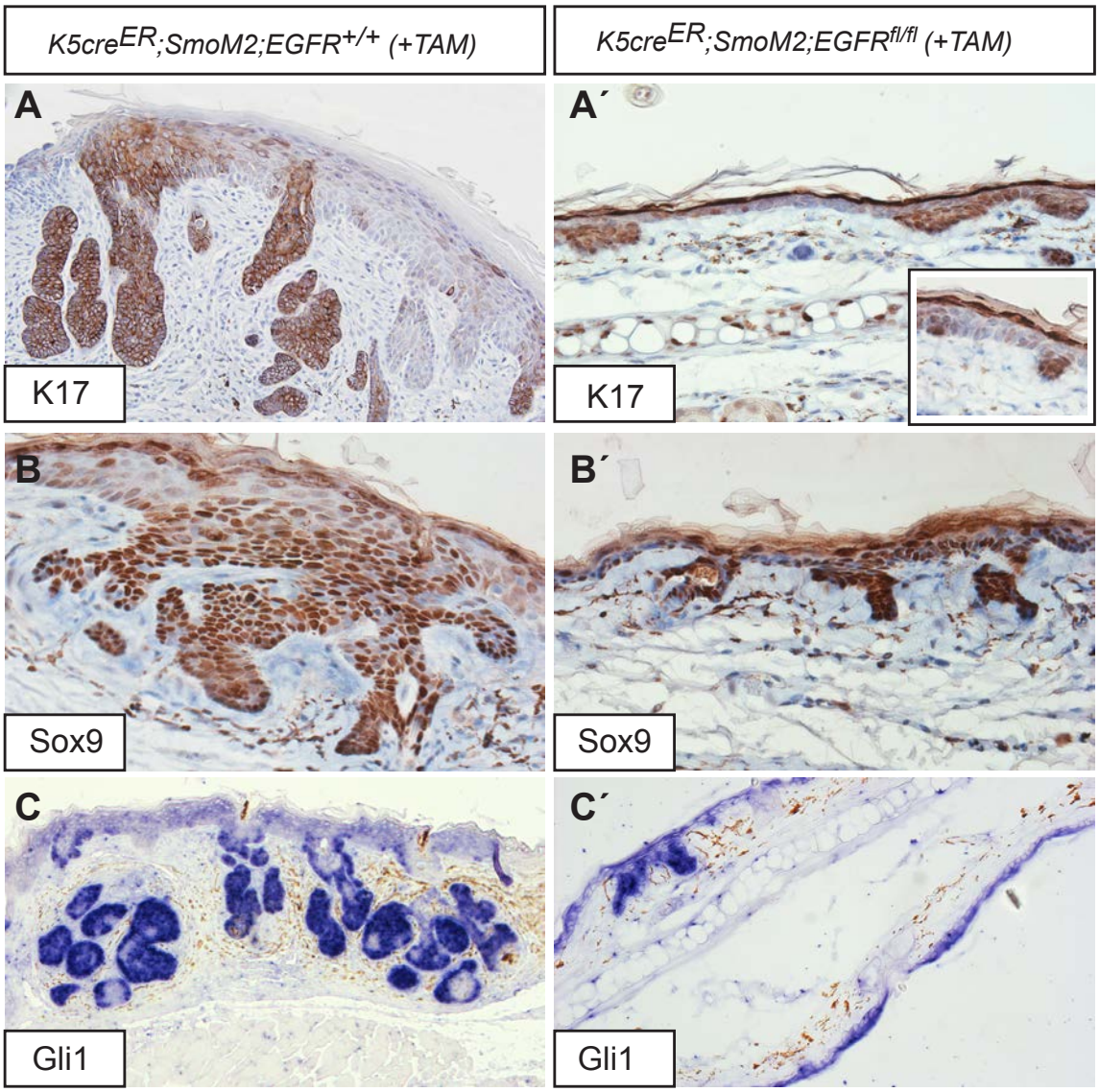

Figure S3: BCC marker expression in SmoM2-induced BCC-like lesions. A-C) Expression of Keratin 17 (K17) (A), Sox9 (B) and Gli1 (C) in tumor lesions of tamoxifen treated (+TAM) *K5cre^{ER};SmoM2;EGFR$^{+/+}$* mice by immunohistochemistry (K17, Sox9) and in situ hybridization (Gli1). A´-C´) Analysis of K17 (A´), Sox9 (B´) and Gli1 (C´) expression reveals BCC-marker expression in residual hyperproliferative lesions of *K5cre^{ER};SmoM2;EGFR$^{fl/fl}$* mice. Inset in A´ shows a K17 positive BCC-like bud.

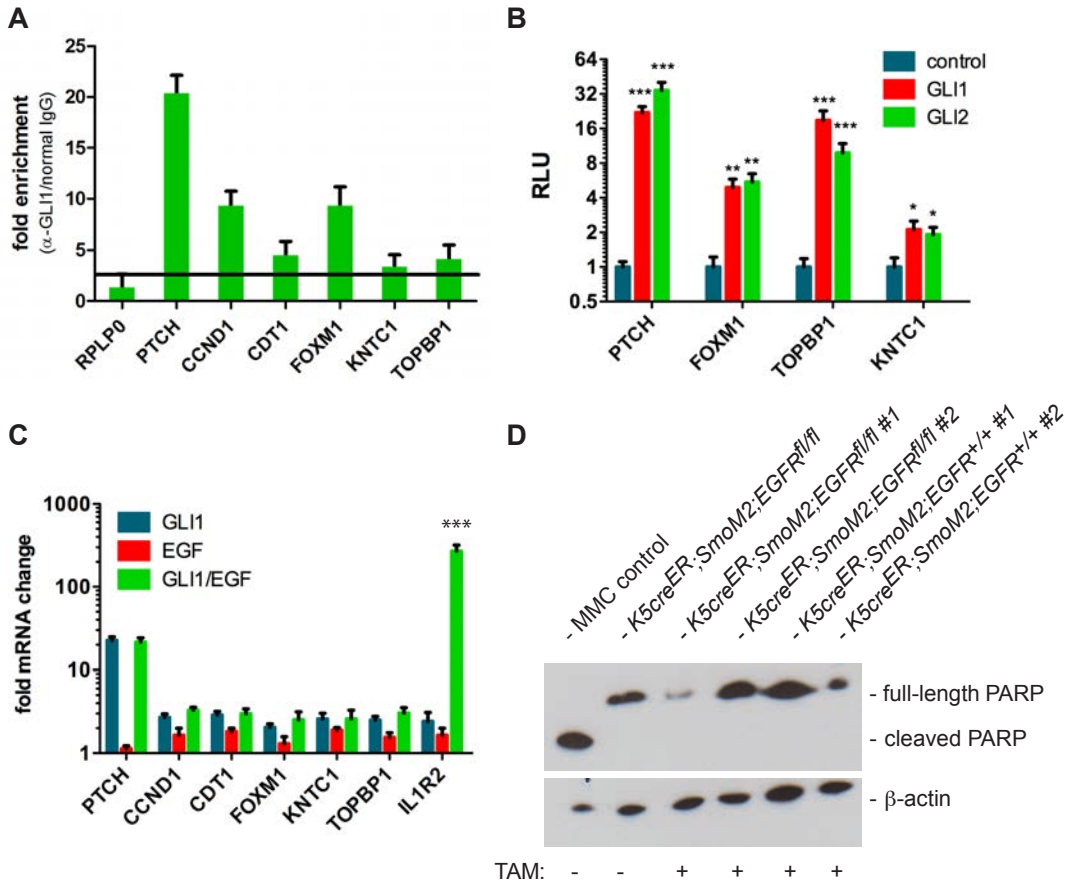

Figure S4: Effect of EGFR-GLI cooperation on direct GLI cell cycle target genes and survival of primary mouse keratinocytes. A) Chromatin immunoprecipitation (ChIP) analysis showing direct binding of GLI1 to the promoters of cell cycle genes including CCND1, CDT1, FOXM1, KNTC1 and TOPBP1. PTCH was used as positive control, RPLP0 as negative control. ChIP experiments were done in human HaCaT keratinocytes. Only genes enriched at least 3-fold by anti-GLI1 antibody are shown (also see Table S2). B) Luciferase reporter assays showing induction of FOXM1, TOPBP1 and KNTC1 promoter activity in response to GLI1 and GLI2 expression. The PTCH promoter served as positive control. Reporter assays were done in 293 cells. C) qPCR analysis showing that the expression of direct cell cycle GLI target genes are not affected by concomitant EGFR signaling. IL1R2 served as positive control for cooperative HH/GLI-EGFR signaling. PTCH induction is shown as EGFR-independent GLI target to demonstrate comparable GLI1 activity in the different samples. Only the EGFR/GLI target IL1R2 (Kasper et al, 2006) showed significant synergistic induction by simultaneous GLI and EGF activation measured 18h post stimulation. D) Deletion of EGFR does not induce apoptosis in primary SmoM2 expressing mouse keratinocytes. Primary keratinocytes of *K5cre^{ER};SmoM2;EGFR$^{+/+}$* or *K5cre^{ER};SmoM2;EGFR$^{fl/fl}$* mice were isolated and analyzed for PARP cleavage to monitor the effect of EGFR deletion on cell survival. Mitomycin C (MMC) treated cells served as positive control, β-actin as loading control. Error bars represent SEM. * = p<0.05; ** = p<0.01; *** = p<0.001; TAM+: keratinocytes isolated from tamoxifen treated mice; TAM-: keratinocytes isolated from untreated mice;

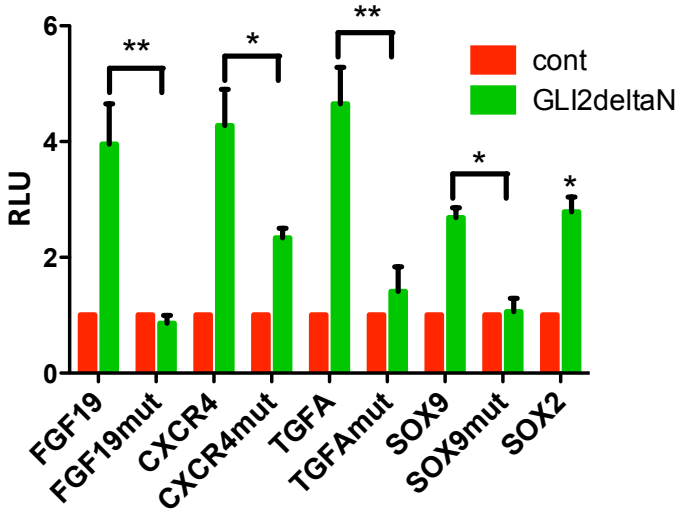

Figure S5: Activation of HH/GLI-EGFR target promoters by active GLI2. Similar to GLI1, expression of a dominant active form of GLI2 (GLI2deltaN) activates the promoters of FGF19, CXCR4, TGFA, SOX9 and SOX2 as monitored in luciferase reporter assays. Reporter constructs were the same as shown in Figure 3C. Error bars represent SEM. * = $p<0.05$, ** = $p<0.01$;

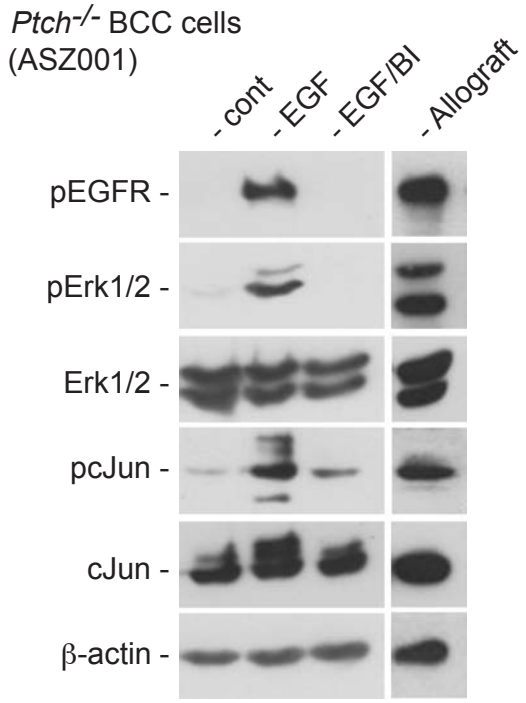

Figure S6: Activation of Mek/Erk/Jun in response to EGFR stimulation in ASZ001 mouse BCC cells. Western blot analysis of Ptch$^{-/-}$ BCC cells treated with EGF or a combination of EGF and the EGFR TKI afatinib/BIBW2992 (BI). In response to EGF treatment, ASZ001 cells show activation and phosphorylation, respectively, of EGFR (pEGFR), Erk (pErk1/2) and Jun (pJun) (lane EGF), which is blocked by the addition of afatinib (0.5µM) (lane EGF/BI). Likewise, ASZ001 BCC cells grafted to nude mice (lane Allograft) display activation of the EGFR/Erk/Jun cascade. Control cells (cont) were treated with solvent only (DMSO).

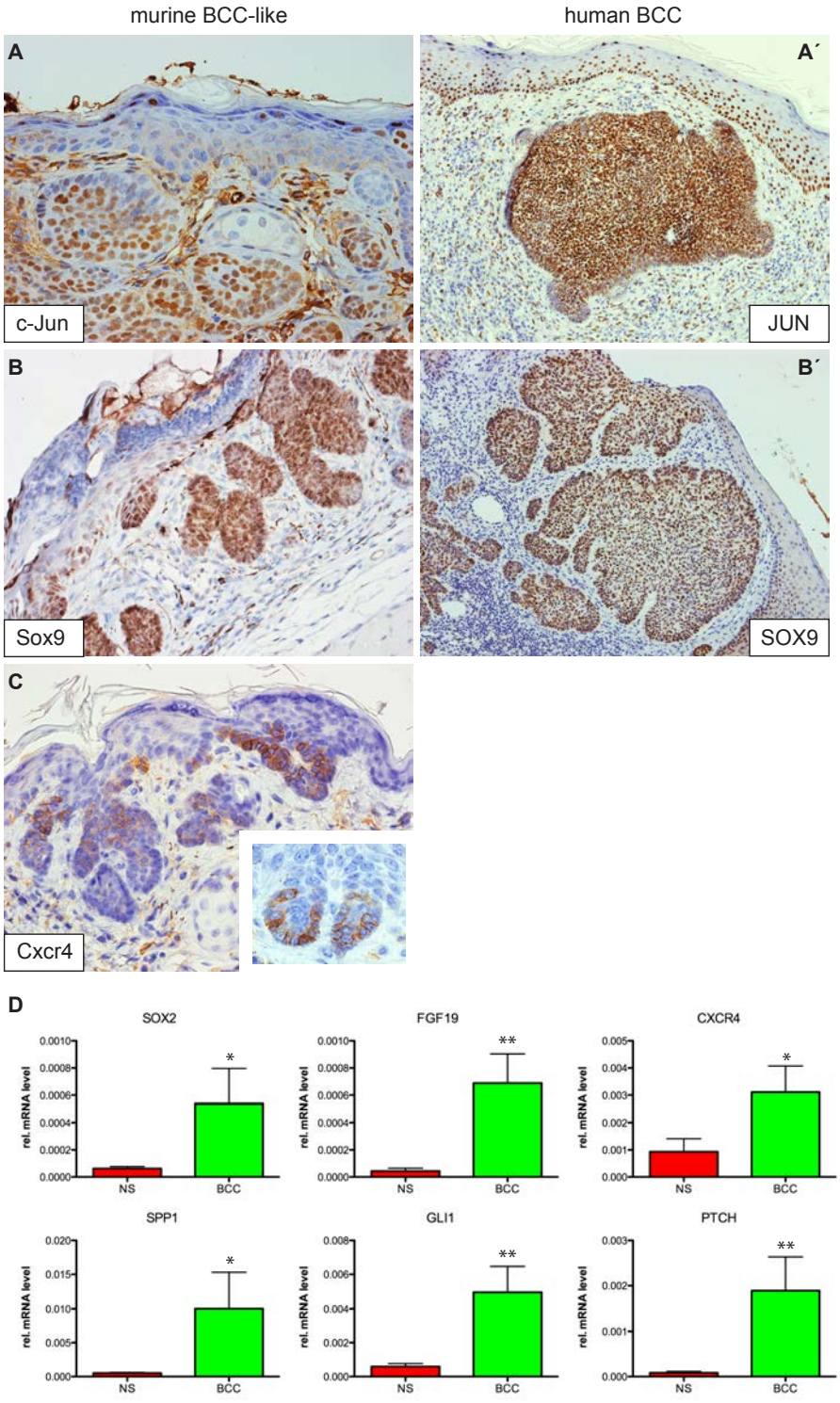

Figure S7: Expression of HH/GLI-EGFR cooperation response genes in mouse and human BCC. A-C) Immunohistochemical analysis of JUN (A), SOX9 (B) and CXCR4 (C) expression in mouse BCC-like lesions of *K5cre^{ER};SmoM2;EGFR$^{+/+}$* mice and human BCC. CXCR4 analysis of human BCC failed due to unspecific background signals. Left images in A, B and C show tumor lesions on the ears of tamoxifen treated mice. Inset in C shows CXCR4 expression at the invasive front of early tumor lesions. D) qPCR analysis of HH/GLI-EGFR response genes SOX2, FGF19, CXCR4 and SPP1 in human BCC samples (n=4) showing increased mRNA expression in tumor lesions compared to normal human skin (NS)(n=3). mRNA levels of the BCC marker genes GLI1 and PTCH are shown as reference and positive control, respectively. Error bars represent SEM. * = $p<0.05$, ** = $p<0.01$;

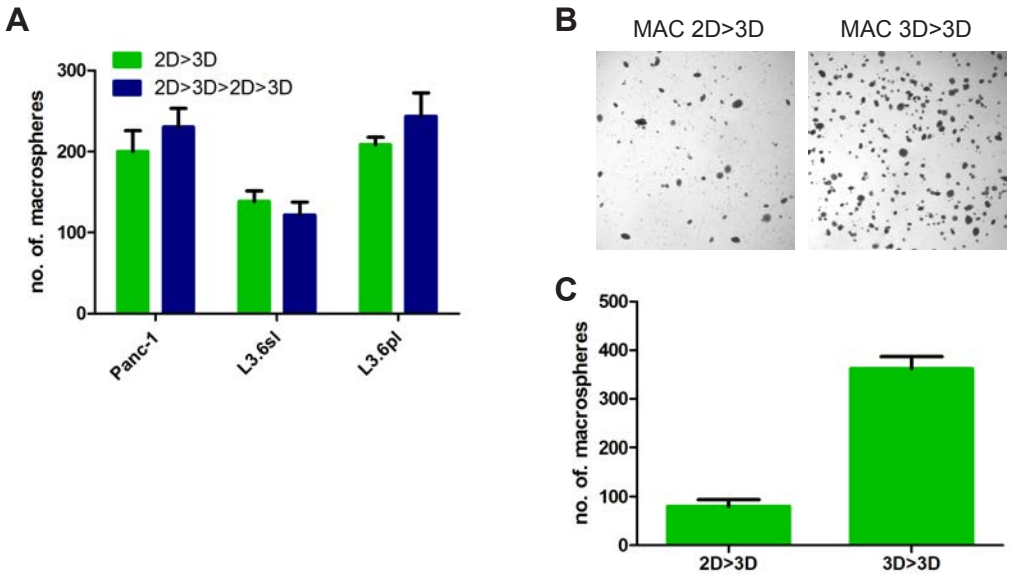

Figure S8: Characterization of tumor-initiating pancreatic cancer cells isolated from 3D cultures. A) The proportion of rare macrosphere-forming cells to cells with low clonogenicity is constant when tumor-initiating macrosphere cells isolated from 3D cultures were passaged in 2D cultures before being re-seeded and grown in 3D cultures. B) By contrast, the fraction of tumor-initiating macrosphere-forming cells is highly enriched if isolated from 3D cultures and directly re-seeded in 3D cultures without intervening growth in 2D cultures. C) Quantification of macrosphere-forming cell experiments shown in B after two serial passages).

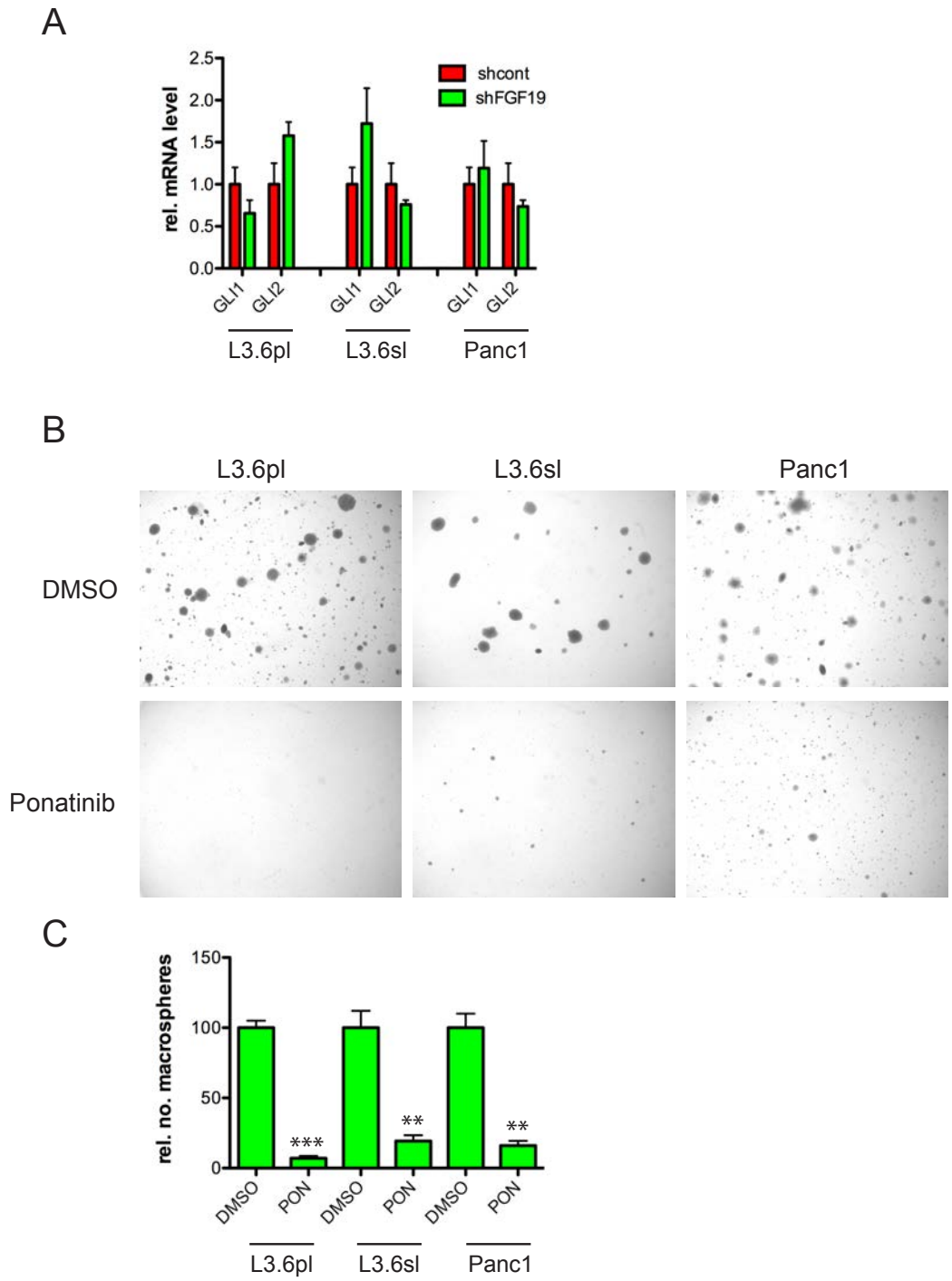

Figure S9: Fibroblast growth factor receptor inhibition inhibits growth of tumor-initiating macrospheres of pancreatic cancer cells. A) qPCR analysis of GLI1 and GLI2 expression in pancreatic cancer cells (L3.6pl, L3.6sl and Panc1) after RNAi mediated knockdown of FGF19 (shFGF19). Control cells were transduced with non-target shRNA (shcont). Inhibition of FGF19 does not significantly affect the expression of GLI1/2 in human pancreatic cancer cells (Student´s t-test $p>0.05$ in all shcont/shFGF19 comparisons). B) Treatment of pancreatic cancer cells (L3.6sl, L3.6pl and Panc1) with the FGFR inhibitor ponatinib (1µM) (*Gozgit et al., 2011) effectively inhibits the formation of macrospheres in 3D cultures. C) Quantitative analysis of the experiment shown in B. Error bars represent SEM. * = $p<0.05$, ** = $p<0.01$, *** = $p<0.001$;

*Gozgit J, Wong, M, Moran L, et al. (2011). Ponatinib (AP24534), a potent pan-FGFR inhibitor with activity in multiple FGFR-driven cancer models with distinct mechanisms of activation. Presented at the 102nd Annual Meeting of the American Association for Cancer Research (AACR) Orlando FL, 05 April 2011. Abstract 3560.

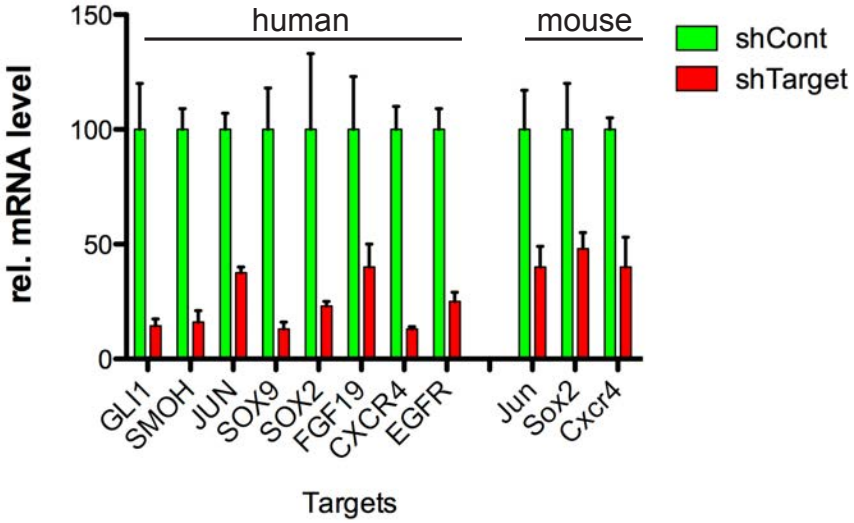

Figure S10: RNAi-mediated knockdown efficiency of human and mouse lentiviral shRNA constructs. For details of the constructs see materials and methods. shRNA mediated knockdown of target mRNAs was determined by quantitative real-time PCR. Target mRNA levels in cells transduced with non-target control shRNA (shCont) were set to 100 and served as reference value for cells transduced with target shRNA (shTarget). Mouse shRNAs were validated in ASZ001 BCC cells, human shRNA contructs in the pancreatic cancer cell lines L3.6sl and Panc-1.